ASTRONOMY
AND
ASTROPHYSICS

The complex radio spectrum of 3C 130

M.J. Hardcastle

Department of Physics, University of Bristol, Tyndall Avenue, Bristol BS8 1TL, UK (m.hardcastle@bristol.ac.uk)

arXiv:astro-ph/9908067v1 6 Aug 1999

Abstract. I present four-frequency radio observations of the wide-angle tail radio galaxy 3C 130. By a technique of simulated observations, I assess the systematic errors in the data due to the varying uv plane coverage in the different observations used. Using spectral tomography I show that, at least in the southern plume, the source can be represented by a two-component model consisting of a flat-spectrum core and steep-spectrum sheath, as recently found in other FRI sources. In addition, there is a strong difference in the high-frequency spectra of the northern and southern plumes. I discuss the implications of these observations for the source's jet dynamics and particle acceleration, and discuss models of the class of WATs as a whole.

Key words: Radio continuum: galaxies – galaxies: active – galaxies: jets – galaxies: individual: 3C 130

1. Introduction

Wide-angle tail radio galaxies are an interesting sub-class of the population of FRI (Fanaroff & Riley 1974) objects, which typically lie at the centres of clusters and show narrow, well-collimated jets which flare abruptly into broad, diffuse plumes. Their radio power is normally intermediate between the more typical jet-dominated FRI and the 'classical double' FRII classes of extragalactic radio source, and an understanding of their dynamics is important to our knowledge of the relationships between these two classes and the possible evolution between them.

In an earlier paper (Hardcastle 1998, hereafter Paper I) I presented new radio maps of the wide-angle tail radio galaxy 3C 130 ($z = 0.109$). Two-frequency spectral index mapping in that paper showed flat-spectrum jets (in this paper, the term is reserved for the narrow, well-collimated features seen in the inner 50 kpc of the sources) and a hotspot (a compact, sub-kpc feature at the end of the northern jet) together with steeper-spectrum material at the edges of the plumes (the broader, more diffuse features seen between 50 and ~ 500 kpc from the nucleus). This steep-spectrum material is particularly clear in the southern plume, and is referred to here as a 'sheath', although I emphasise that, unlike the sheaths seen in some twin-jet FRI

radio galaxies, this region has no polarization properties to distinguish it from the rest of the plume. The sheath is the only feature of the two-point radio spectrum which is not obviously consistent with a fairly simple model for the source's dynamics, in which particles are accelerated at the base of the plumes and the spectral steepening along the plumes is a consequence of outflow of an ageing electron population. The additional data presented here show that the situation is more complicated than that simple model would imply.

B1950 co-ordinates are used throughout this paper, and spectral index α is defined in the sense $S \propto \nu^{-\alpha}$.

2. Data

The X-band (8.4-GHz) and L-band (1.4-GHz) data used in this paper were described in Paper I. Data from a short (0.5 h) C-band (4.9-GHz) observation with the NRAO Very Large Array (VLA) in its C configuration, taken on 1984 Jun 11, were kindly provided by Alan Bridle. The U-band (15-GHz) images presented here are the result of a 3-hour observation with the VLA in its D configuration taken on 1999 Mar 11. All data were reduced and analysed using the AIPS software package.

2.1. Flux scales

As described in Paper I, both 3C 48 and 3C 286 were used as primary flux calibrators for the L- and X-band observations, which were taken between 1994 Nov 10 and 1995 Nov 28. Specifically, 3C 286 was used for the A-configuration X-band observations and 3C 48 for all others. The data analysis in Paper I used the older version of the SETJY AIPS task, which incorrectly rounded coefficients in the analytic expression for the flux densities of calibrator sources. However, the effect is very small when combined with the change between the old (1990) values of the coefficients and the more appropriate new (1995.2) values. L-band fluxes should be reduced by 0.3% and the X-band B, C and D-configuration fluxes by 2%; the A-configuration X-band flux, based on 3C 286, should be reduced by 2.5% when the effect of the partial resolution of the source is incorporated, but we use 2% for all the X-band data in what follows. The primary flux calibrator for the C-band observations was 3C 48; the fluxes derived from this are increased by 2%

to take account of the variation in 3C 48's flux density between the epoch of observation and 1995 (Perley & Taylor 1999). The primary flux calibrator for the U-band observations was 3C 48, and it is assumed that 3C 48 has not varied significantly between 1995 and 1999, so that the flux densities derived from this are correct.

2.2. Mapping

The long, multi-array X- and L-band observations of Paper I sample the uv plane more densely and have a much broader range of baselines than the short, single-configuration C-band observations. The U-band observations are long and so well-sampled, but still cover a narrow range of baselines. In order to try to correct for this and ensure that fluxes from maps were directly comparable I mapped the source at all four frequencies with the CLEAN-based AIPS task IMAGR using only baselines between 1.8 and 50 kλ; the uv plane was acceptably sampled in this range at all four frequencies, though the C-band data are still sparse (Fig. 1). Reweighting the data (using different values of the 'robustness' parameter in IMAGR) ensured that the fitted beams were similar. The same 4.0-arcsec restoring Gaussian was then used for each map, scaling residuals appropriately. (Experiment showed that, in spite of folklore to the contrary, there was no significant difference between the results of this procedure and those of restoring clean components with the Gaussian which was the best fit to the dirty beam and then convolving to the required resolution.) Primary beam correction was applied with the AIPS task PBCOR. Small shifts were applied to each image so that the unresolved cores were aligned to better than 0.05 arcsec.

3. Results

3.1. Images and their fidelity

Images of 3C 130 at the four frequencies used are shown in Fig. 2.

Some apparent evidence of anomalous spectral behaviour can immediately be seen from these maps. For example, the inner jets of the source appear fainter at 5 GHz than they do at 8.4 GHz, implying an inverted spectrum; this would be very surprising in an extended source region. However, since the uv plane coverage is sparsest at long baselines in the 5-GHz data, these apparent spectral differences may simply be a result of image infidelity. The CLEAN algorithm can be viewed as an attempt to interpolate over the missing spacings in the uv plane, but image fidelity clearly depends on the amount of interpolation needed.

To examine the degree to which image infidelity was a problem in these datasets, I made a test model of the source (consisting of 100,000 CLEAN components from an 8-GHz map with all baselines < 50 kλ). Using the AIPS task UVSUB, I replaced the real data in all four datasets with the Fourier transform of the CLEAN component model; this simulates the effect of observing an identical source with different uv coverage. The four simulated datasets were then mapped with

IMAGR. The ratios of fluxes in the resulting maps indicates the fidelity with which a particular component is likely to be reproduced. While the L- and X-band datasets produce very similar maps of the model data, the U-band sampling seems to underestimate the flux of the southern jet, and the C-band sampling gives a noticeably poorer reproduction of the original model, with regions of lower flux particularly in the jets and at the edges of the plumes.

I next made another model, consisting of 100,000 CLEAN components from a similar 1.4-GHz map. The 1.4-GHz data has denser sampling in the centre of the uv plane. Simulating observations of this model with the uv coverages of the four datasets shows that even the X- and U-band datasets do not perfectly reproduce structure on the largest scales; the effect is to produce spurious spectral 'steepening' at the very edges of the plumes, increasing the spectral index by 0.2–0.3 at the edges of detectability. The steep-spectrum sheath, however, is too strong an effect to be entirely or mostly due to this undersampling. But these results illustrate the danger of the common assumption that simply matching resolutions or longest and shortest baselines will give maps that are safe to use for spectral index analysis. All spectra at the very edges of the plumes, the U-band spectra of the jets, and the C-band data throughout the source, must therefore be treated with caution.

As an experiment, I tried making a map of spectral index between the 5-GHz data and the 8.4-GHz data remapped with the 5-GHz sampling. Assuming that the original 8.4-GHz images have ideal fidelity, we might expect this resampling to compensate fully for the poor sampling of the 5-GHz data. Although sampling the 8.4-GHz data sparsely does reduce the flux in the jets, the resulting 5–8.4-GHz spectral index is still very flat (0.1) while the spectral indices in the plumes are much more reasonable. This suggests that even identical sampling does not give completely reliable results for snapshot observations.

3.2. Flux densities and spectra

Flux densities of the various components of the source are tabulated in Table 1. Except for the core and hotspot flux densities, which were derived from a fit of Gaussian and zero level using the AIPS task JMFIT, these were measured from polygonal regions defined on the 15-GHz map using MIRIAD. In Fig. 3 the resulting component spectra are plotted.

The spectra of the core, jets and northern plume are not unexpected. There is some slight evidence for a steeper spectrum in the N jet between 8 and 15 GHz, perhaps indicating a cutoff in the spectrum of the jet at high frequencies, but it is possible that the N jet is affected by undersampling. The S jet is certainly somewhat affected by undersampling at 15 GHz. The N plume shows a slightly concave spectrum, suggesting the presence of multiple spectral components. The hotspot in the N plume shows a flat spectrum with $\alpha \approx 0.5$, consistent with a model in which it is produced by particle acceleration at the shock at the end of the N jet; its spectrum has only steepened slightly by 15 GHz.

The immediately striking result of these measurements is the steep spectral index between 8 and 15 GHz in the southern plume. We can be sure that this is not an artefact of poor sampling; the S plume lacks compact structure, and simulations show that we would not expect any flux on the scales of the observed emission to be missing from the 15-GHz maps. It appears that there is a genuine break in the spectrum between 8 and 15 GHz in the southern plume which is not present in the northern plume. As shown in Fig. 4, this effect is not limited to a single region in the plume, but is visible throughout.

The steep-spectrum 'sheaths' around the plumes, particularly the southern plume, which were visible in the 8-GHz data presented in Paper I, are missing in the 15-GHz images, although again simulated images show that the 15-GHz observations have sampling which should be adequate to reproduce them. This implies that the sheath regions have very steep spectra between 8.4 and 15 GHz. Using regions defined with MIRIAD on the 1.4–8.4-GHz spectral index map, in which the sheath region is well defined, I find that $\alpha_{8.4}^{15} \gtrsim 2$ for the sheaths around both north and south plumes, whereas $\alpha_{1.4}^{8.4} \sim 1$.

4. Discussion

4.1. Tomography and the nature of the steep-spectrum 'sheath'

It has recently been suggested (e.g. Katz-Stone & Rudnick 1997) that the jets in some FRI radio galaxies have a two-component structure, consisting of a flat-spectrum 'core jet' and steep-spectrum surrounding 'sheath'. Katz-Stone et al. (1999) show that the same picture may apply to two WAT sources from the sample of O'Donoghue et al. (1990). The observed spectral steepening with distance from the core in FRI sources might therefore be unrelated to spectral ageing and expansion, as is frequently assumed; it might simply be a consequence of the increasing dominance of the sheath component.

To test whether such a picture is viable in 3C 130, I constructed a spectral tomography gallery as discussed by Katz-Stone & Rudnick; this involves generating a set of maps by subtracting a scaled version of the high-frequency map from the low-frequency map, so that for each pixel of the tomography map (I_t) we have

$$I_t(\alpha_t) = I_l - \left(\frac{\nu_h}{\nu_l}\right)^\alpha I_h$$

where α_t is varied. Features of a given spectral index vanish on the tomography map corresponding to that spectral index; if the apparent steepening in 3C 130 is due to varying blends of a flat- and steep-spectrum component, and the steep-spectrum component is relatively smooth, the plumes should appear more uniform in a tomography map with a spectral index corresponding to that of the flat-spectrum component, as the flat-spectrum component should then have vanished, leaving only a (scaled) version of the steep-spectrum component. If there is no single, uniform flat-spectrum component, the plumes will still show structure for any value of α_t.

The full gallery of tomography images is not shown, but Fig. 5 shows a representative example, made with the L and X-band maps taking $\alpha_t = 0.55$. It will be seen that the jets and N hotspot are oversubtracted, giving rise to negative flux densities on the tomography map – this is as expected, since their spectral index is about 0.5 (Paper I). In the N plume, there is still considerable structure in this image, but the S plume has a much more uniform surface brightness after subtracting the flat-spectrum component, suggesting that a two-component model of the source is close to being adequate here. This is further illustrated in Fig. 6, which shows the results of spectral tomography on slices across the S plume; these show that, at least within 1.5 arcmin of the core, the plume can be modelled as a superposition of a flat-spectrum component with $\alpha \sim 0.55$ and a broader steep-spectrum component with $\alpha \sim 1.2$, with the flat-spectrum component becoming progressively fainter with distance along the plume; this is consistent with the results of Katz-Stone et al. (1999). The spectrum of the flat-spectrum component, as estimated from the spectral index at which it disappears on tomography slices, appears to have steepened by 105 arcsec from the core; this is true even after a rough correction is applied for the effects of the undersampling of the X-band data on large spatial scales (as assessed in section 3.1).

The situation is certainly more complicated in the N plume, where there is in any case less evidence for a steep-spectrum sheath in the spectral index maps of Paper I; if a two-component model is to be viable there, it must allow for some spatial variation in the spectrum of the flat-spectrum component. But this would not be surprising, since there is much stronger evidence for ongoing particle acceleration in the N plume. I return to this point below.

If there are two spectral components, what is the origin of the steep-spectrum material? Katz-Stone & Rudnick identify several possibilities for the sheath in 3C 449. There may be a two-component jet, with the steep-spectrum material only becoming visible at a flare point; or the steep-spectrum material may have evolved from the flatter-spectrum component through ageing, adiabatic expansion, diffusion into a region of lower magnetic field or a combination of these. Without additional low-frequency observations it is impossible to say whether the injection spectral indices of the two components are the same, so we cannot rule out a two-component plume in 3C 130. But it is certainly also possible that the sheath has evolved from the flatter-spectrum component. Modelling of the synchrotron spectrum does not allow me to rule out any of the possibilities; the sheath may be substantially older than the flat-spectrum jet, or it may be of comparable age and in a weaker magnetic field, or a combination of the two. It is possible to say that the two regions cannot simultaneously be in local energy equipartition and be the same age if they have aged in the same B-field.

In any case, it is clear that the steepening of the overall spectrum of the plumes with distance from the source, as discussed in Paper I, is better modelled in terms of a two-component spectral model than in terms of spectral ageing along the jet.

4.2. The high-frequency spectra of the plumes

The striking difference between the high-frequency spectra of the N and S plumes (Fig. 4) is unusual in radio galaxies, particularly in a source as symmetrical at low frequencies as 3C 130. It is, of course, possible that the symmetry is illusory and that for some reason the electrons in the S plume are moving much more slowly, and therefore appear to be ageing much more rapidly, than those in the N plume. However, it seems more likely that the spectral difference is related to particle acceleration in the plumes.

In the S plume, there is no clear evidence in any single-frequency map or in the polarization maps for a compact hotspot like the one seen in the N of the source. The two-frequency spectral index maps presented in Paper I show the flat-spectrum S jet penetrating the S plume for some distance, but do not show any particularly flat-spectrum termination region; the best candidate region was in the area of maximal surface brightness at ~ 40 arcsec from the core. From those data it seemed possible that there was a hidden compact hotspot, perhaps suppressed by Doppler beaming, and that the particle-acceleration situations in the two plumes were nevertheless symmetrical. But the 15-GHz data taken together with the absence of a hotspot suggest a model in which there is currently little or no shock-related particle acceleration in the S plume, and consequently no shock-related termination of the jet. The steep 8.4–15-GHz spectrum is inconsistent with continuous injection models for the electron spectrum. If we assume for the ageing B-field the equipartition field of 0.46 nT used in Paper I, and (as in that paper) use a Jaffe & Perola (1973) aged electron spectrum then we can estimate the time for which particle acceleration must have been turned off to produce the observed spectrum of the southern plume (Table 1) from an initially power-law spectrum with $\alpha = 0.5$, as observed in the northern hotspot; it is of order 5×10^7 years. This is an appreciable fraction of the commonly assumed lifetime of a radio source, but it is strongly dependent on the assumed ageing B-field. (Note that, because the region of flux measurement is defined on 15-GHz maps, the plume spectrum used here is essentially that of the flat-spectrum component discussed above, and does not include a contribution from the steep-spectrum sheath.)

5. Speculations on source models

If there is no explicit jet termination, how does this fit in with models for WAT formation? We can clearly see a well-collimated jet entering the southern plume. By analogy with the jets in FRIIs we believe this jet to be supersonic, and numerical modelling (e.g. Norman et al. 1988, Loken et al. 1995) has suggested that to make a WAT a shock should form at the end of the jet, giving rise to the characteristic flaring at the base of the plumes; in any case, we should see *some* evidence for a transition between the supersonic jet and the diffuse, trans-sonic plume. But there is no evidence for a jet-termination shock either in the form of a hotspot as in the northern plume, as

discussed in Paper I, or in particle acceleration, as discussed above. How, then, does the southern jet terminate?

Perhaps the most attractive model is one in which the southern jet currently does not terminate, while the northern jet in 3C 130 is currently impinging on the edge of the source, causing a shock (Fig. 7); the terminations of both jets are *dynamic* and move about in the base of the plume, and it is only when one intersects with the plume edge that we see a shock and associated particle acceleration. Simply from the small-scale deviations from linearity seen in high-resolution maps of the jets, we know that the point at which the jet enters the plume must vary with time. In FRII radio galaxies, numerical simulations have shown (e.g. Norman 1996) that the working surface can move about as a result of turbulence in the cocoon. In WATs, bulk motions in the X-ray emitting medium on scales comparable to those of the jets may provide another source of jet buffeting.

This sort of model for 3C 130 seems incompatible with a picture in which the flaring of WAT plumes is caused by propagation across a shock in the external medium (Norman et al. 1988) or into a crosswind (Loken et al. 1995), because in these models we would expect to see hotspots on both sides at all times. The latter model is in any case hard to reconcile with the straight plumes seen in 3C 130 and in some other sources which are morphologically WATs (Paper I). Instead, it may be the case that WATs of 3C 130's type are the natural result of the action of the external medium on a low-power FRII source.

The pressure in the lobes of an FRII is expected to fall with time (e.g. Kaiser & Alexander 1997, eq. 20) and if it falls below the thermal pressure of the external medium, the lobes can no longer be supported and will begin to collapse. The natural result is a breaking of the source self-similarity and a slow crushing of the cocoon, which begins with the region closest to the centre, where the thermal pressure is highest (cf. Williams 1991).[1] In many FRII sources, X-ray observations show that the thermal pressure from the external medium is greater than the minimum pressure in the radio lobes; only the very smallest sources seem to be unambiguously overpressured. Cocoon crushing is therefore a viable process. Once the radio lobes have been squeezed away from the nucleus, asymmetries in the thermal atmosphere, together with buoyancy effects, can account for the large-scale distortions in the lobes seen in many low-power FRII galaxies (Williams 1991). But, if the environment is suitable, there seems to be no reason why buoyancy cannot drive this process further in particular sources, pushing the lobes further and further away from the centre. The detailed shapes of the sources this would produce would depend on the advance speed of the front of the lobe, but if the lobes were pushed out far enough we would start to see WAT-like objects,

---

[1] This picture differs from the model discussed by Katz-Stone et al. (1999), in which WATs are the remnants of FRIIs in which the jets have turned off, and in which cocoon crushing is the force that renders the source WAT-shaped. The detection of localised, compact hotspots which are clearly overpressured with respect to the surrounding emission, and must therefore be assumed to be transient features being supplied with energy by the jet, seems to rule that picture out.

provided that the jets continued to terminate at the end of the lobe nearest the centre. At intermediate stages we would see objects like NGC 326 (Worrall et al. 1995), which differs from a WAT only in that its tails are slightly recessed from the termination of its jets. The evolutionary sequence from FRII to WAT is represented in Fig. 8. The bending of WAT tails on large scales can still, of course, be understood in terms of bulk motions of cluster gas.

If true, this model would imply that we do not expect to see very young (small) WATs; they all evolve from FRIIs and need a certain amount of time (dependent on jet power and properties of the external medium) to do so. It is certainly the case that the WATs studied by O'Donoghue et al. (1993) show a range of core–'hotspot' distances that begins around 20 kpc and is much smaller than the range of core–hotspot distances seen in classical doubles. What is not clear is whether the timescales of the processes needed to push the lobes of radio galaxies out beyond the jet termination are short enough to be active here. More detailed information on the environments of WATs will become available with the launch of *Chandra* and *XMM*; it will need to be coupled with detailed, fully three-dimensional simulations of jets in realistic atmospheres to answer all the outstanding questions on the dynamics of these sources.

References

Fanaroff B.L., Riley J.M., 1974, MNRAS, 167, 31P
Hardcastle M.J., 1998, MNRAS, 298, 569
Jaffe W.J., Perola G.C., 1973, A&A, 26, 423
Kaiser C.R., Alexander P., 1997, MNRAS, 286, 215
Katz-Stone D.M., Rudnick L., 1997, ApJ, 488, 146
Katz-Stone D.M., Rudnick L., Butenhoff C., O'Donoghue A.A., 1999, ApJ, 516, 716
Leahy J.P., Bridle A.H., Strom R.G., 1998, Internet WWW page, at URL: <http://www.jb.man.ac.uk/atlas/>
Loken C., Roettiger K., Burns J.O., 1995, ApJ, 445, 80
Norman M.L., 1996, in Hardee P.E., Bridle A.H., Zensus J.A., eds, Energy Transport in Radio Galaxies and Quasars, ASP Conference Series vol. 100, San Francisco, p. 319
Norman M.L., Burns J.O., Sulkanen M.E., 1988, Nat, 335, 146
O'Donoghue A.A., Owen F.N., Eilek J.A., 1990, ApJS, 72, 75
O'Donoghue A.A., Eilek J., Owen F., 1993, ApJ, 408, 428
Perley R.A., Taylor G.B., 1999, VLA Calibrator Manual, available at URL <http://info.aoc.nrao.edu~gtaylor/calib.html>
Williams A.G., 1991, in Hughes P.A., ed., Beams and Jets in Astrophysics, Cambridge University Press, Cambridge, p. 342
Worrall D.M., Birkinshaw M., Cameron R.A., 1995, ApJ, 449, 93

Table 1. Flux densities of components of 3C 130

Region	Flux (mJy)			
	1.4 GHz	4.9 GHz	8.4 GHz	15 GHz
Core	16.2 ± 0.1	27.4 ± 0.1	27.8 ± 0.05	27.6 ± 0.3
Hotspot	41.8 ± 0.2	24.8 ± 0.2	17.3 ± 0.1	11.5 ± 0.6
N jet	15.7 ± 0.2	(5.2 ± 0.1)	5.70 ± 0.03	3.4 ± 0.2
S jet	11.1 ± 0.3	(2.4 ± 0.1)	3.95 ± 0.04	1.1 ± 0.2
N plume	715 ± 0.8	267 ± 0.3	172.1 ± 0.1	124 ± 0.5
S plume	623 ± 0.7	220 ± 0.3	153.1 ± 0.1	59 ± 0.5

Figures in brackets are considered to be seriously affected by the sampling problems discussed in the text.
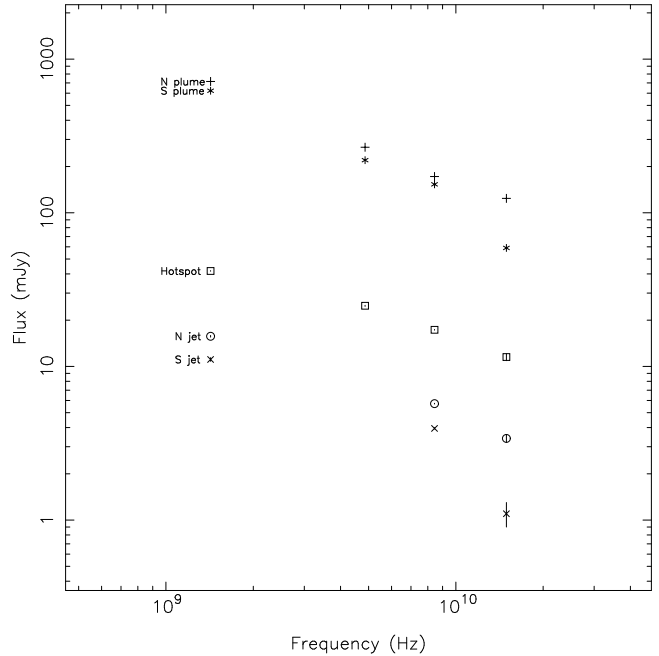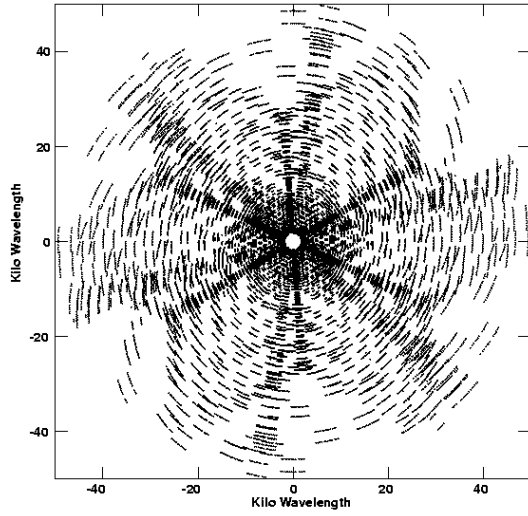

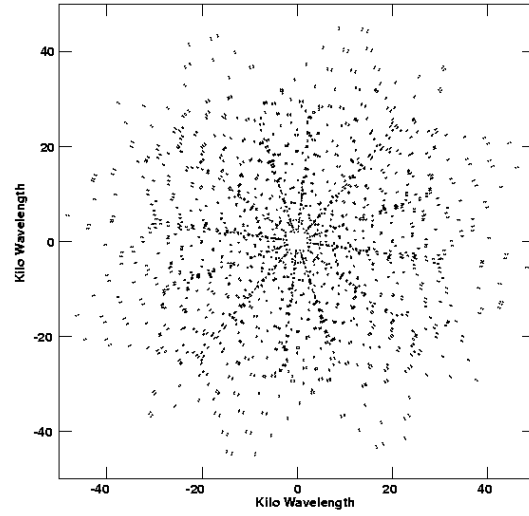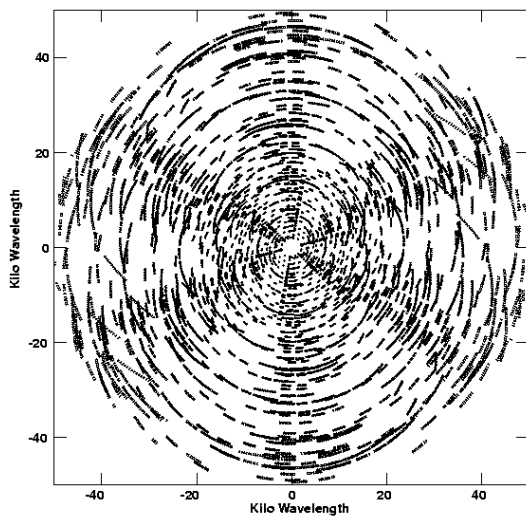**Fig. 3.** Flux densities of the components of 3C 130 plotted against radio frequency.

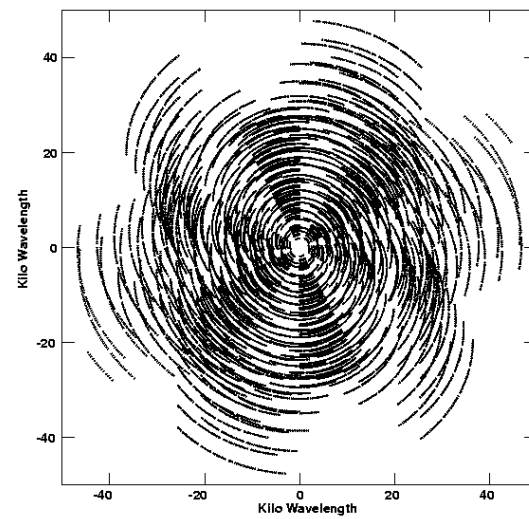1.4 GHz (L band)   4.9 GHz (C band)

8.4 GHz (X band)   14.9 GHz (U band)

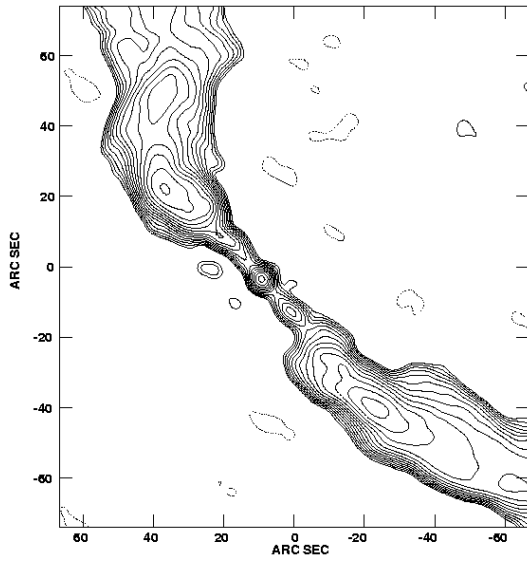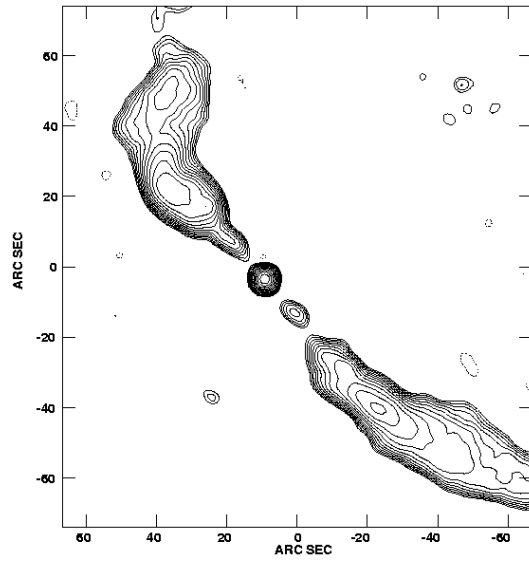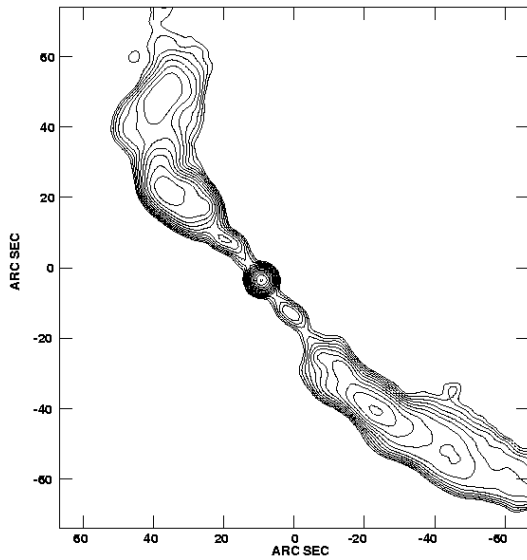**Fig. 1.** uv plane coverage for the four datasets for baselines between 1.8 and 50 kλ.
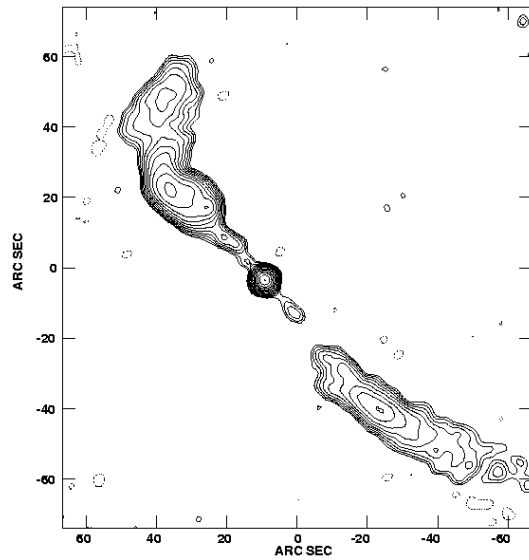
1.4 GHz (L band); $300\sqrt{2}$ μJy beam^{-1}

4.9 GHz (C band); 300 μJy beam^{-1}

8.4 GHz (X band); 300 μJy beam^{-1}

14.9 GHz (U band); 300 μJy beam^{-1}

Fig. 2. 4-arcsec resolution maps of 3C 130 at the four frequencies, made with data between 1.8 and 50 kλ. The base contour levels are listed below each map; contours increase logarithmically by factors of $\sqrt{2}$ at each step. Negative contours are dashed.
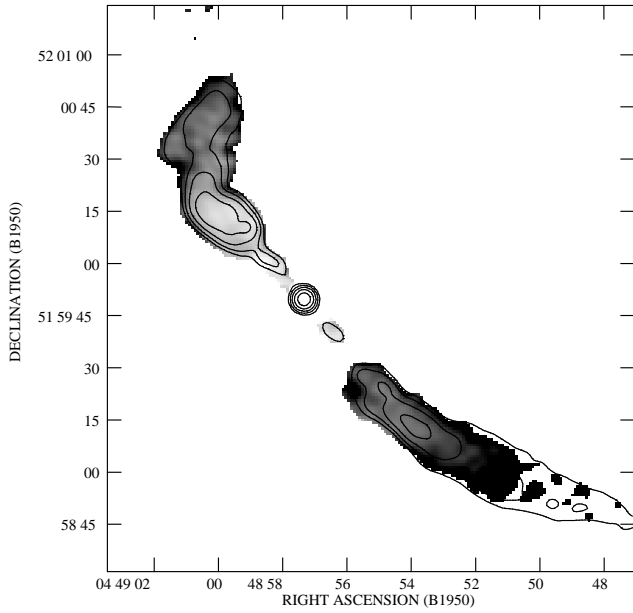
Fig. 4. The spectral index of 3C 130 between 1.4 and 15 GHz. Linear greyscale between $\alpha = 0.5$ (white) and $\alpha = 1.2$ (black). Only points with fluxes greater than the 3σ level on each map are shown. Overlaid are contours of the 4-arcsec resolution map of 15-GHz emission at $1, 2, 4 \ldots$ mJy beam^{-1}.
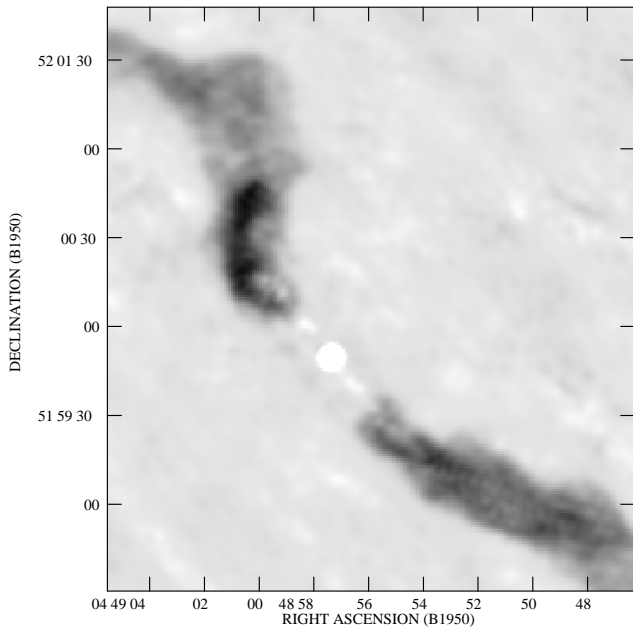

Fig. 5. A tomography slice between 1.4 and 8.4 GHz with $\alpha_t = 0.55$

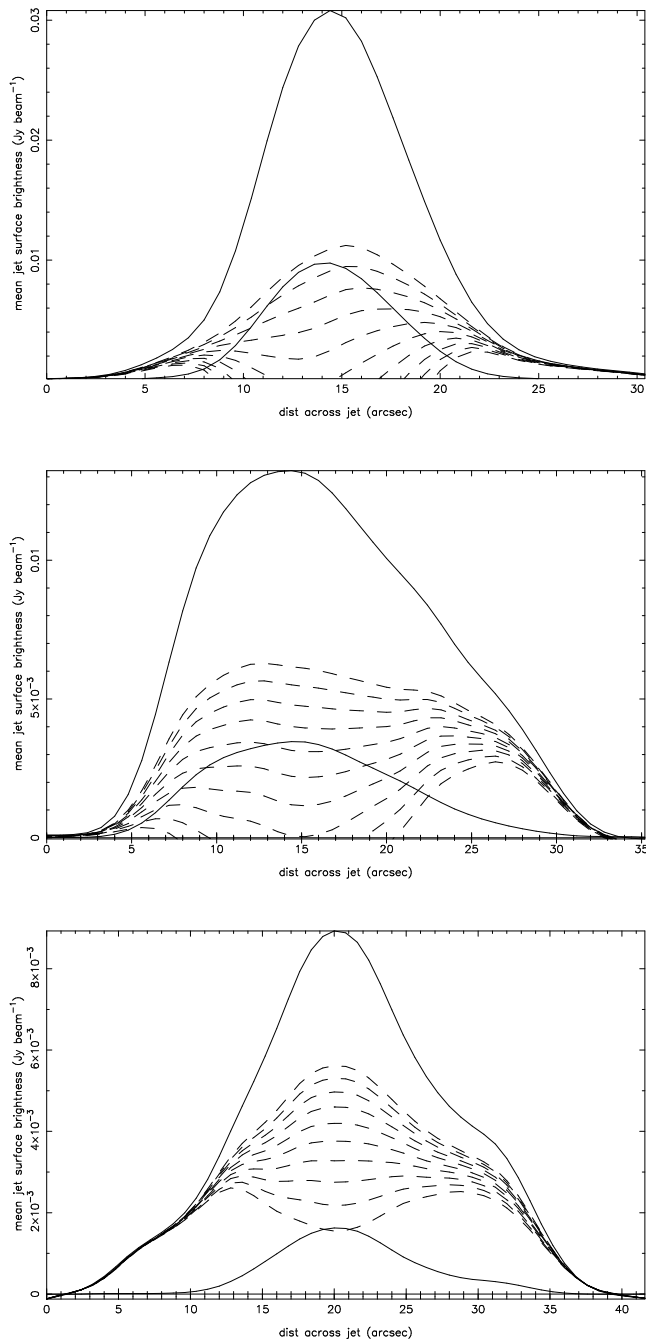**Fig. 7.** Schematic of the possible current situation in 3C 130.

Fig. 6. Tomography slices across the S plume taken at (from top) 40 arcsec, 75 arcsec and 105 arcsec from the core. The solid lines show the surface brightness as a function of distance across the plume (integrated along 8-arcsec strips) at 1.4 GHz (upper line) and 8.4 GHz (lower line); the dashed lines show the results of tomographic subtraction, starting at the top with $\alpha_t = 0.4$ and proceeding in steps of 0.05 in spectral index. Note that for the nearer two slices the most uniform surface brightness after subtraction is given by $\alpha_t = 0.5 - 0.6$. For the furthest slice the best tomographic spectral index appears steeper.
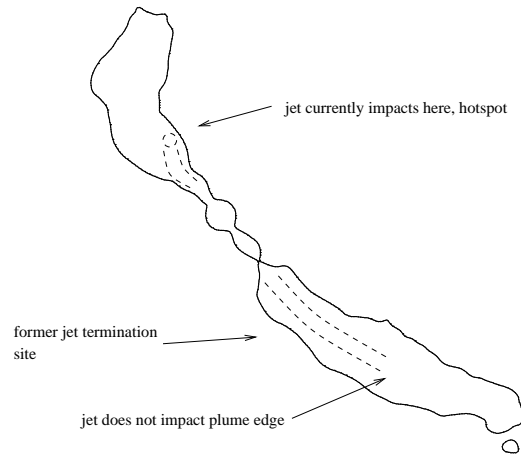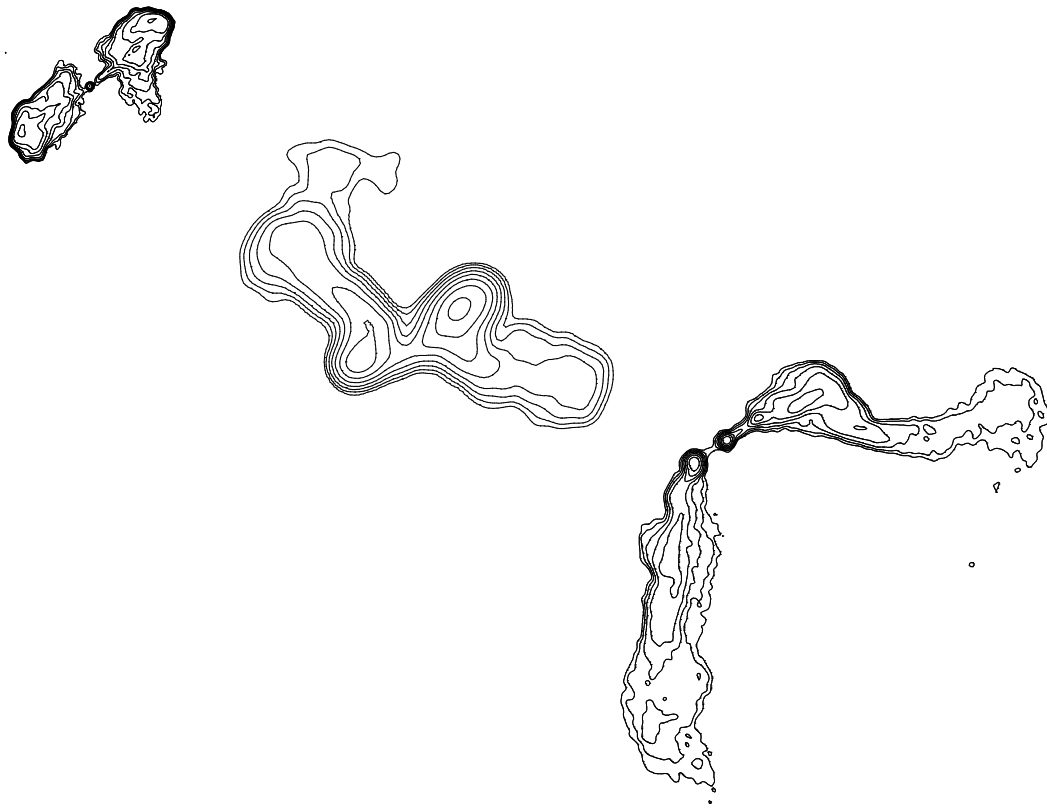
Fig. 8. An 'evolutionary sequence' of double objects in clusters. Top left (3C 438): cocoon crushing has driven the radio emission away from the axis at the centre, backflow is deflected. Middle (NGC 326): outflow is in 'tails' flowing sideways, perhaps bent by buoyant forces. Bottom (3C 465): the lobes have merged with the tails to form plumes; bulk motion in the cluster gas bends them. All maps are VLA images at ~ 1.4 GHz. 3C 438 and 3C 465 are taken from the 3CRR atlas (Leahy et al. 1998); the image of NGC 326 was supplied by Mark Birkinshaw.